Journal of Hydraulic Structures
***J. Hydraul. Struct.*, 2018; 4(1): 36-54**
DOI: 10.22055/JHS.2018.24985.1075

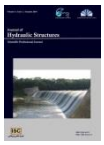

OPEN ACCESS

Ocean Currents Modeling along the Iranian Coastline of the Oman Sea and the Northern Indian Ocean

Morteza Jedari Attari[1]
S. Abbas Haghshenas[2]
Arash Bakhtiari[3]
Mohammad Hossein Nemati[4]

Abstract

The Makran Coast (Iranian Coastline of the Oman Sea on the Northern Indian Ocean) plays an important role in country's future navigation and trade due to its accessibility. In 2014, the Iranian Makran coastline was selected by the PMO to be studied as the Phase 6 in the series of Monitoring and Modelling Studies of Iranian Coasts with all disciplines being in investigated including currents. All previously measured current data (in 2006, 2007 and 2008) along the Makran coastline showed an oscillating (reversing) alongshore currents with no detectable dominant frequency. The oscillation period of these currents varies approximately from 3 days to a week. The most significant objective of this study was to simulate the oscillating behaviour of the Makran coastal currents. In this regard, the global oceanic current pattern over the Northern Indian Ocean was simulated using a 3-dimensional non-structured model and comparisons with the data from several global resources have been made. The model was calibrated using the available vertical current profile data along the coastline.

Keywords: Ocean Currents, Circulation Patterns, Numerical Modelling, Oman Sea

Received: 18 February 2018; Accepted: 08 May 2018

1. Introduction

The southeast coast of Iran bordering the western Makran region is exposed to the Indian Ocean (see Figure 1) and is directly affected by the climate and hydrodynamic processes of this ocean [1]. Measurements of currents by the Port and Maritime Organization (PMO) [2] in 2006-7 around Chabahar and by the Iranian Fishery Organization (IFO) [3] in 2008 at Zarabad, have

[1]Visiting Researcher, Institute of Geophysics – University of Tehran, Iran.
[2] Institute of Geophysics – University of Tehran, Iran, Email: sahaghshenas@ut.ac.ir (**Corresponding author**)
[3] 3)Project engineer, Middle East Water and Environment Co., Tehran, Iran.
[4] 4)Iranian Ports and Maritime Organization, Tehran, Iran.

shown the presence of oscillating ocean currents along this coastline. These currents reverse every 3 days to a week. They are typically strong through the water column with the near-bed current velocity reaching up to 0.5 m/s at 20~30 m depth.

Figure1. Study area

The Indian Ocean (especially at the northern hemisphere) is under effects of two distinct climate conditions. In the winter monsoon, strong winds blow from the North-West and head towards South when they reach to Somalian Coastline. In the summer monsoon, the direction totally reverses and winds blow from the South-West heading straight towards Makran Coastline [4]. Consequently the major ocean currents of the northern Indian Ocean such as Somali Current gradually develop and strengthen and eventually disappear twice a year trying to adjust themselves with the wind.

Even though oceanic currents (in the Indian Ocean) have been investigated by several researchers, the influence of global oceanic currents on Makran coastal currents has not been probed so far. Figure 2 was illustrated by NASA [5] using an assimilative model representing the North Indian Ocean currents. As it appears in the figure, except for the two East-West elongated regions which are indicated by blue boxes, the rest of the ocean carries strong and dynamic currents.

In analogy to the mentioned fact, Lopez et.al [6] were focusing in the Bay of Bengal and developed a global model for the Northern Indian Ocean setting the open boundary at S20 Tropic. Their model's grid size was 0.5 degree and 38 vertical layers was applied in their model which adequately was able to simulate the Bay of Bengal currents.

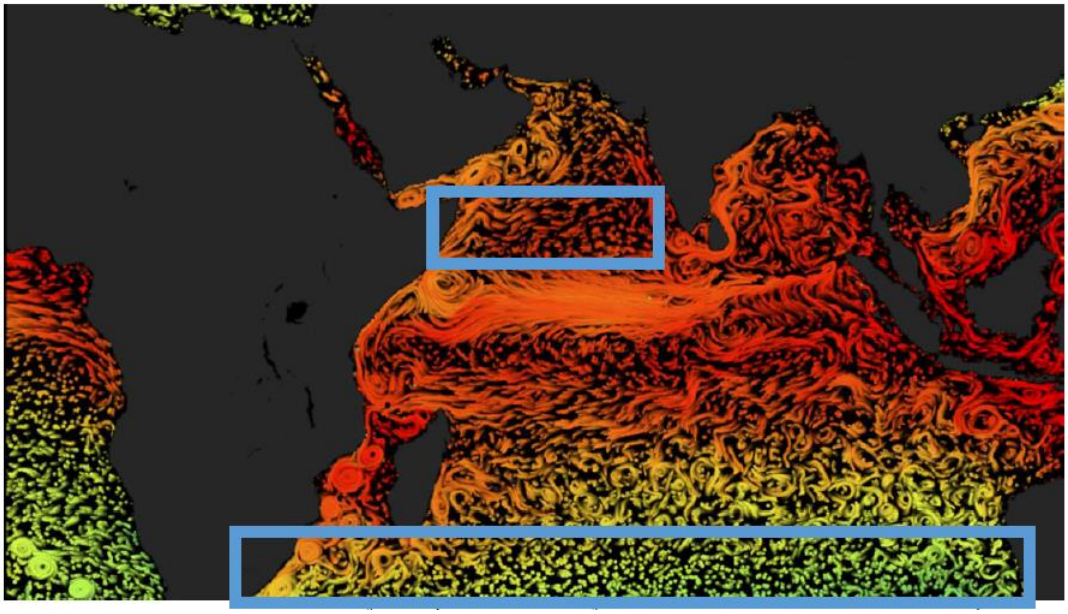

Figure2. The North Indian Ocean Currents

According to Aneesh [7] (based on a modelling results), the accuracy of model results, significantly enhances by considering the water level variations at the southern boundary at S30 Tropic along with density variations in a 3D model. In another attempt by Kurian & Vinayachandran [8], in a model with a same domain and a grid size of 0.25 degree, in spite of setting the open boundary at 30S Tropic as a closed wall, the model results did not affected at the Indian Coasts. Kawamiya and Oschlies [9] also obtained the desirable results with a similar domain. L'Hégaret [10] applied a semi-local HYCOM model to the similar domain and compared the results to the observed ARGO data [11] inside the domain which showed a good consistency. It is noted that he used the data from the global HYCOM model [12] as the initial and open boundary condition.

According to the literature review, it is concluded that, it is necessary to adopt a 3-dimensional baroclinic model in order to simulate the oceanic currents along the coastlines of the Oman Sea including the Makran Coasts.

2. Measured data

Figure 3 shows all the data locations which were gathered and extracted for calibration and verification purpose in this study. An invaluable data set recorded during the first phase of the monitoring projects (by PMO) [2] includes current profile measurements in 25 m depth at a location outside Chabahar Bay. Measurements at this location cover the period from September 2006 until early June 2007 immediately after the Cyclone Gonu event. The oscillating ocean currents have been captured in this data set. The deployed current profiler device (i.e. bottom-mounted AWAC) also recorded water temperature near the seabed. A number of tide gauges deployed inside and outside of Chabahar Bay measured the water level. The location of the current profiler AW2 is E60.65 N25.26 and Tis tide gauge (TG1) located at E60.594 N25.35. Figure 4 illustrates the current rose of recorded data by AW2.

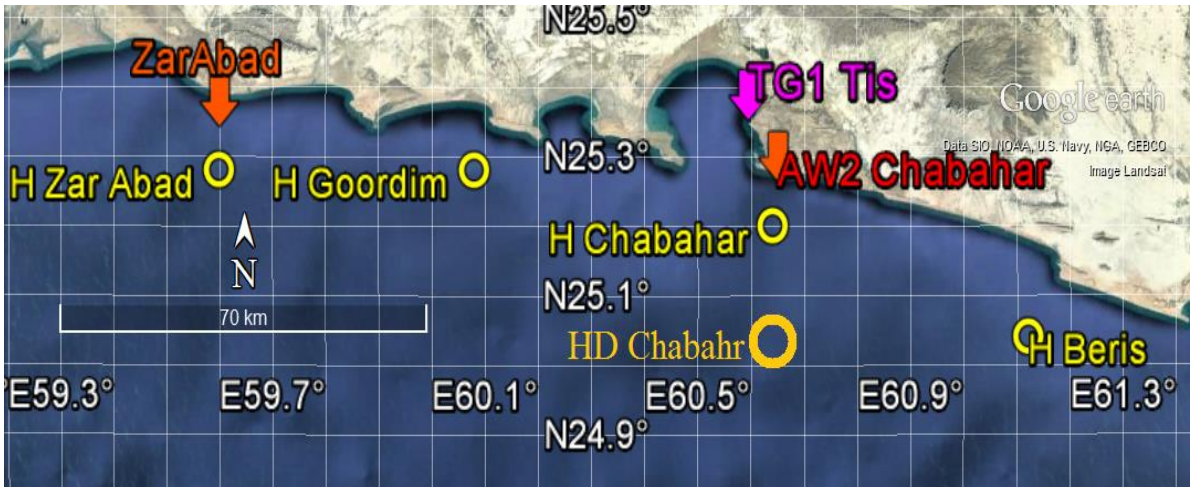

Figure3. Locations of the data collection stations

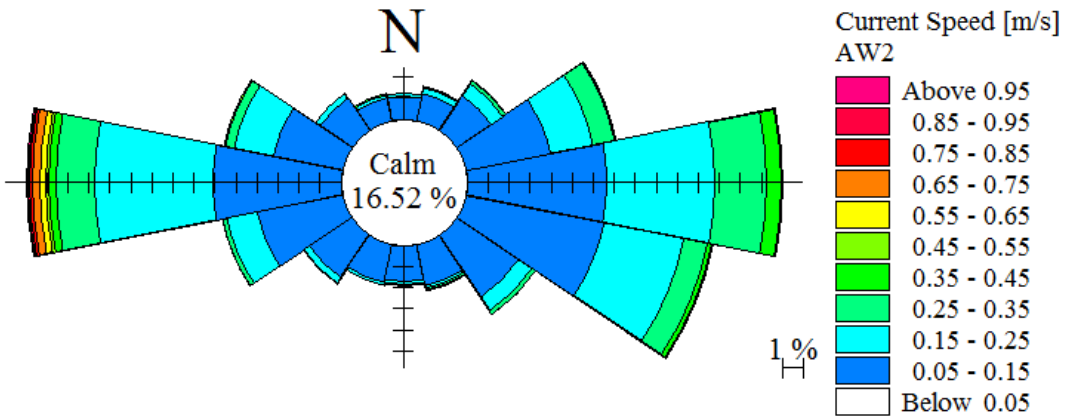

Figure4. AW2 data current rose

In 2008 another bottom mounted AWAC (in 19 m depth) was deployed at ZarAbad vicinity (E59.6 N25.28) by IFO [3]. Similar patterns of current direction in this 4-month-long data (July to October) indicated that the mentioned pattern of oscillating currents dominates the Makran coastline.

In addition to the measured current data which fall in the shallower edge of the continental shelf, daily surface current, water level, and temperature data from global HYCOM [12] assimilative global model developed by the USACE in collaboration of NASA, NOAA and several universities worldwide, were also collected for the last three months of 2006 to be used for evaluating the model performance in the deeper areas. The data is available at 1/12 degree spatial resolution.

3. Methodology

Due to importance of geostrophic currents and the relatively deep water conditions in the Makran area, a 3-dimensional hydrodynamic model had to be used for proper simulation of oceanic currents.

MIKE3 by DHI software has been adopted in order to investigate the currents and sea level variations. The ability of this model in resolving geostrophic processes was investigated through applying the model to a well-known experiment described by Tartinville, et al. [13]. The domain is a 20 m deep and 30 km × 30 km open sea region. The latitude was chosen as 52° N and hence the Coriolis parameter is set to 1.15×10^{-4} s^{-1}. The horizontal grid resolution is 1 km and 20 vertical levels were used. In the centre of the domain, a 10 m deep, 3 km radius cylinder of relatively freshwater is placed in the upper layer. Simulations are performed for 144 hours without any bottom or surface stress. They approved that IFREMER and Delft3D models' results are in consistency with the observed values. Comparing the model results with the data and other already approved 3-dimentional hydrodynamic model results showed that MIKE3 is acceptably capable of resolving 3D geostrophic oceanic currents (Figure 5).

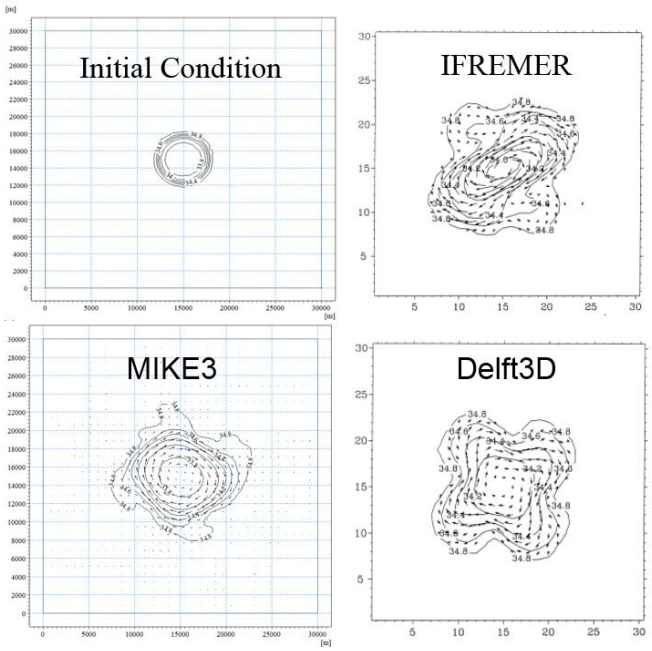

Figure5. Sea surface salinity and velocities through the center of the central eddy at the beginning and end of the experiment. Top left panel: Initial condition, Top right panel: IFREMER Model, Bottom right panel: Delft3D model, Bottom left panel: MIKE3 model

4. Numerical modeling

Simulations started from the beginning of 2006 to allow model warm up and convergence of the temperature field. The last four months of 2006 was selected for the model calibration period. Required initial and boundary conditions data for currents, water level, and temperature fields were obtained from publicly available sources such as Global Ocean Physical Reanalysis System (C-GLORS) [14]. The wind and pressure field data obtained from European Centre for Medium-Range Weather Forecasts (ECMWF) which then implemented in WRF model in order to increase the accuracy by adding meso-scale equations [15]. The global wind field have a coarse resolution of 0.25 degree and a time step of 6 hours, the wind field provided [6] for this simulation has 0.1 degree spatial resolution and the time step of 1 hour. Considering the

temperature variations in the model implies the need for air temperature, short and long wave radiation data as well. Also, sea surface change data was obtained from CCAR [16].

Finding the most appropriate model configuration that can properly simulate large scale oceanic processes was a matter of trial and error. Applying various domains showed that obtaining reasonable results requires adopting a domain far larger than the study area boundaries. The mesh size, number and form of vertical layers also play a significant role in the validity of the model results. Eddy permitting grid resolution of 0.3 degree was selected for the ambient oceanic domain while the grid size decreases to 0.01 degree (≈1 km) near the Makran area. Figure 6 shows the final selected model domain which extends to the southern hemisphere. The bathymetry data was obtained from ETOPO1 [17] which is combined to the existing local hydrography data provided by PMO.

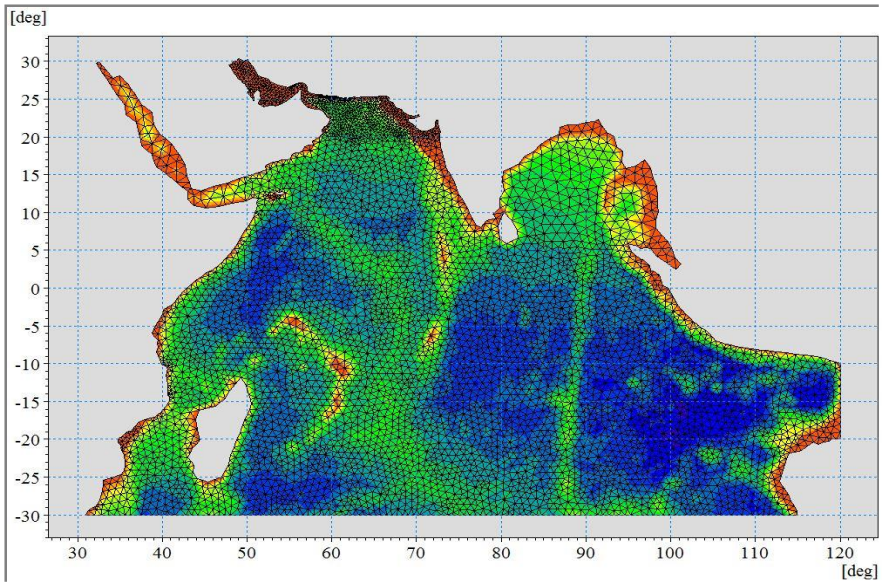

Figure6. Computational domain

In the middle of the Indian Ocean, water depth reaches to approximately 5000 m. Therefore a combined vertical layer grid was used. 10 sigma layers at the surface followed by 47 Cartesian layers in the deep ocean. This configuration ensures well utilizing the sigma layer ability in accurate water level change calculations as well as avoiding the deficiency of sigma layer in resolving the large depth differences and steep slopes where its supposedly almost horizontal interfaces has to place almost vertical at ocean edges and around underwater mounts which results in fatal numerical divergences.

Computational time step of 120 s revealed to be small enough which below that, no changes appeared in the results. Although as a deep ocean model, the global current field is not sensitive to bed roughness, comparisons on the results and data from current profilers in the shallower edge of the continental shelf (AW2 and ZarAbad) showed that model results are more consistent when the parameter was set 0.002 m.

Table 1 presents a summary of distinguishing features of some model calibration versions. It is noted that except for cc_N20_01 and cc_N10_03 which the southern boundary was placed at N20 and N10 Tropics, respectively, the rest of the models has a Southern boundary at S30 Tropic and an Eastern boundary at E120 Mercator. In order to avoid repeating the similar characteristics of calibration models, only the changed parameter is mentioned in front of each

model version, i.e., if a feature mentioned for a model at above row is not mentioned in the next row implies that the feature is duplicated from above and no changes have been made in that regard.

Three Groups of models with the large domain appear in Table 1. Models titled cc_S30_03's major feature is having closed boundary while to others, i.e., cc_S30_12s and cc_S30_14s use C-GLORS current and temperature data along with CCAR data for surface elevation at the open boundary. cc_S30_12s group uses the standard mesh (sea Figure 6) while the latter group uses a mesh which its grid size in the vicinity of Makran area is divided in half.

Small and medium domains are not capable of reproducing the real patterns in the currents of Makran. The reason is that, the open boundary in those models is too close to the area of being concerned and because there was no accurate data available to apply at the boundary, we had to set it as a close boundary or use 1-month averaged 3-D current data from C-GLORS which obviously is not appropriate for that purpose. Never the less C-GLORS 1-month averaged current and temperature field data was used for the initial condition of the model which because of considering an 8-month warm up period, the results were not affected. In the larger domain however, most of the oceanic gyers which affect the Makran Coastline are reproduced within the domain and the effect of far located open boundaries conditions fades out.

The numerical scheme for resolving the vertical eddy viscosity plays a significant role in the model performance. Trying k-epsilon turbulence scheme resulted in intensified stratification which separates a thin film of warmer water layer at the surface dragged intensely by the wind force while the rest of the vertical column remains detached from the governing forces and as a consequence colder than recorded temperature and mostly stagnant. On the other hand, log-low formulation represents milder stratification in the simulations, resulting in better consistency both for current direction at the surface and temperature at the bottom layer. It should be noted that, wind friction parameter significantly affects the results.

Table1. Model Calibration Versions Characteristics.

Model	Features
cc_N20_01	Small Domain & Open Boundary Condition (OBC) = closed boundary & Vertical Eddy Viscosity (VEV) = log-law & Wind Friction (WF) = 0.0026 & Initial Water Level Condition (IWLC)= uniform zero & Initial Current Filed (ICF) = stationary & Vertical Temperature Dispersion (VTD) = 0 & Horizontal Temperature Dispersion (HTD) = 0, & No Evaporation
cc_N10_03	Medium Domain
cc_S30_03	Large Domain
cc_S30_03_01	With Computed Evaporation
cc_S30_03_02	VEV = k-epsilon
cc_S30_03_03	WF = varying linear (0.0012~0.0024)
cc_S30_03_04	WF = varying linear (0.0017~0.0024)
cc_S30_12	OBC = S30: level CCAR and free currents, E120: level CCAR and currents from C-GLORS & VEV = log-law & WF = 0.0026 & IWLC = CCAR & ICF = C-GLORS
cc_S30_12_01	VEV = k-epsilon
cc_S30_12_02	WF = 0.0022
cc_S30_12_03	WF = 0.0019
cc_S30_12_04	VEV = log-law & WF = 0.0030
cc_S30_12_05	WF = 0.0040
cc_S30_12_06	VEV = k-epsilon & WF = 0.0026 & VTD = 1
cc_S30_12_07	HTD = 1

cc_S30_14	fine mesh & VEV = log-law & WF = 0.0026 & VTD = 0 & HTD = 0
cc_S30_14_01	VEV = k-epsilon & WF = 0.00245 & VTD = 1 & HTD = 1
cc_S30_14_02	VTD = 1.5
cc_S30_14_03	VTD = 3
cc_S30_14_04	VTD = 4.5

Three variables have been investigated in an analytical analysis in order to detect the most appropriate model setting. Summaries of comparisons with HYCOM data at four points located at 100 m depth and one point at 600 m depth (sea Figure 3) for surface u-velocity component, v-velocity component and temperature appear in Figure 7, 8 and 9 respectively.

Same approach has been adopted in order to investigate the ability of the model in simulation of recorded data by AW2. Figure 10 represents summaries for correlation coefficient (CC) and root mean square of errors (RMSE) for three mentioned variables. It is noted that the temperature recorded by AW2 stands for sea bottom temperature (in contrary to HYCOM data which belong to surface).

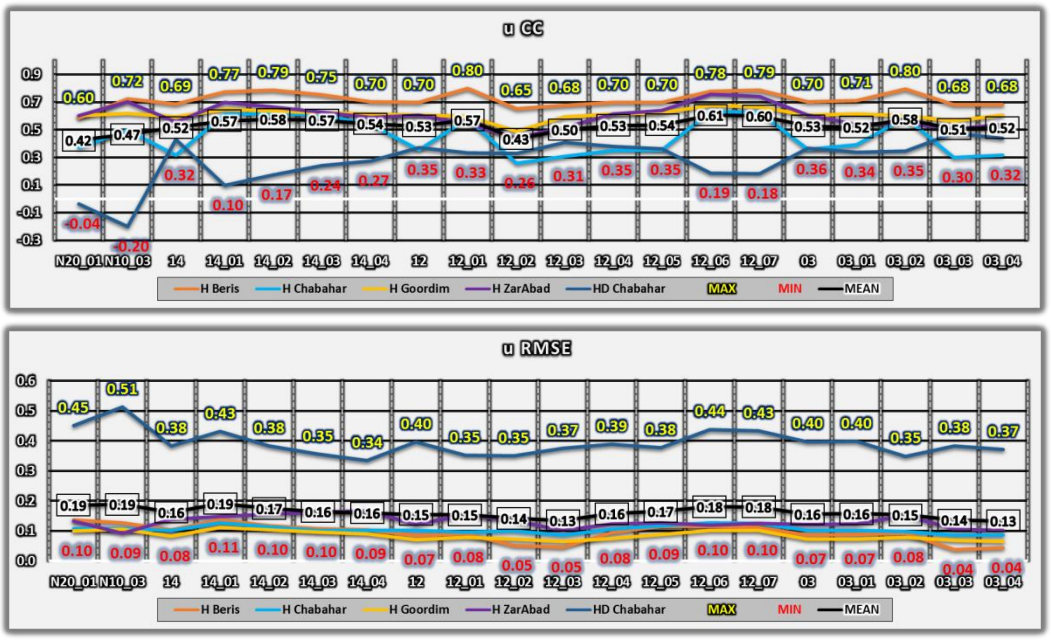

Figure7. Correlation coefficient and RMSE of surface u-velocity component for model results and HYCOM data

Another major role playing variable on this decision is, the water level variation. Using a closed boundary at the lateral openings of the model seems that does not affect the current or temperature filed while it has a significant influence on water level variation. The comparisons on model results and the surge filtered from the tide gauge at Tis (TG1) showed that applying CCAR 7-day averaged sea surface data at the model boundary extremely enhance the model accuracy. The data from the tide gauge (Tis) was filtered applying a Fast Fourier transform and the surge was obtained. The model results at the location of the tide gauge extracted and compared to the data which is shown in Figure 11. The model accurately simulates the arising surge due to Cyclone Gonu. It is noted that the results from cc_S30_03 were shifted 0.2 m

upward in order to fit the data while the results from cc_S30_12_04 are already in consistency with the observed levels.

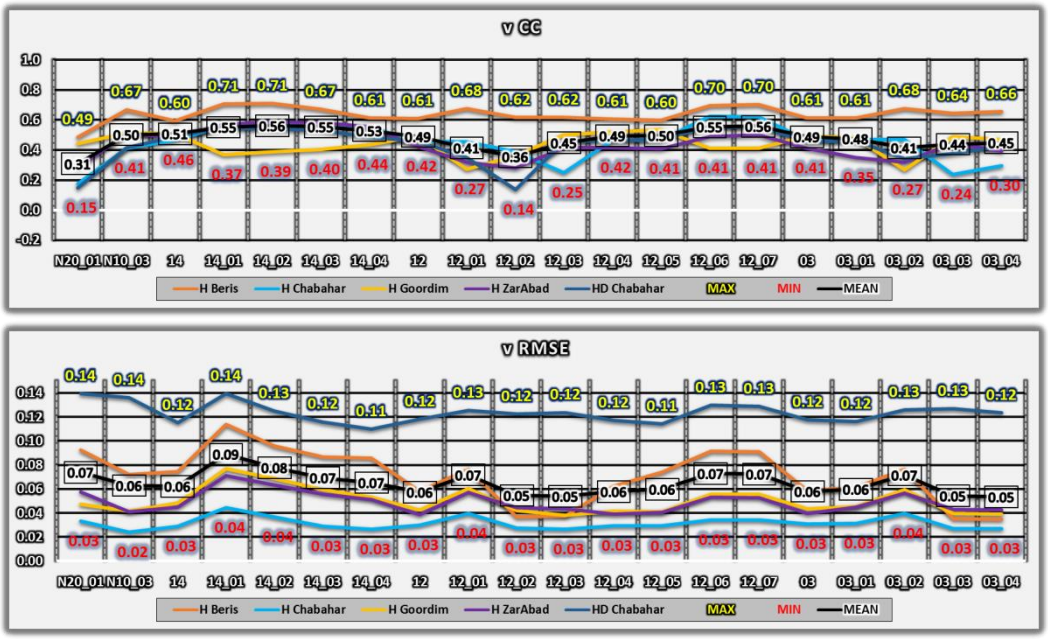

Figure 8. Correlation coefficient and RMSE of surface v-velocity component for model results and HYCOM data

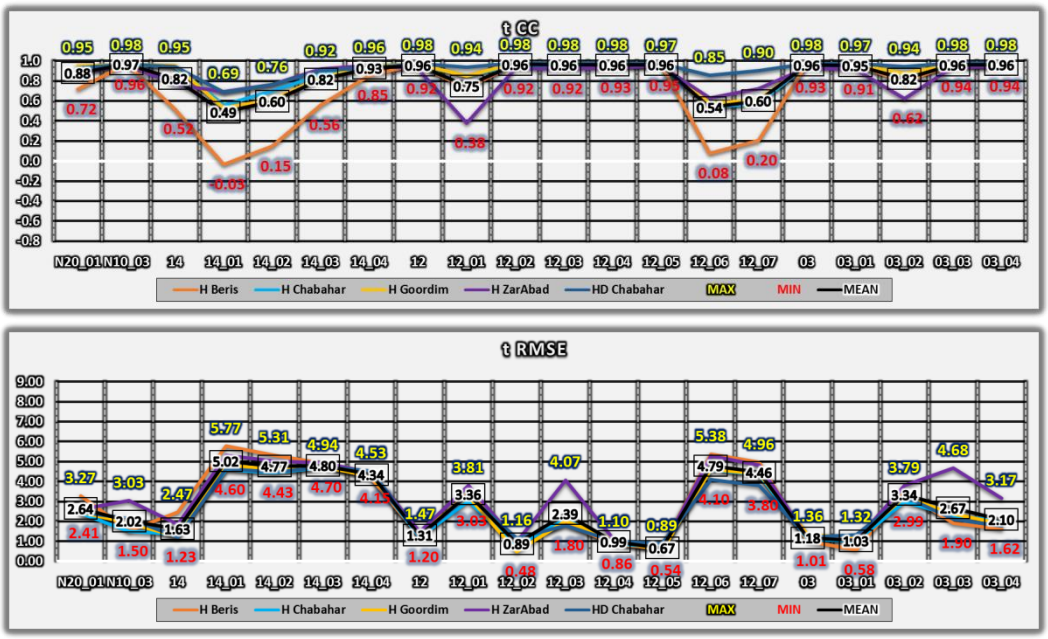

Figure 9. Correlation coefficient and RMSE of surface temperature for model results and HYCOM data

Analytical analysis revealed that using cc_S30_12_04 provides the best results. It is also revealed that decreasing the grid size in spite of having a devastating effect on computational time/cost does not improve the model results.

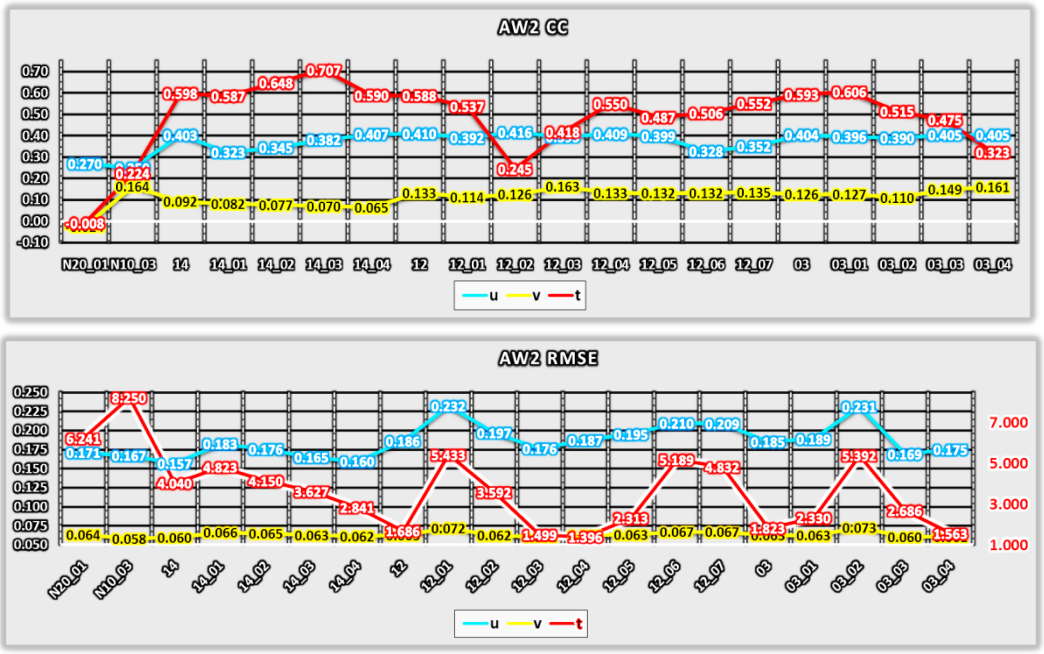

Figure 10. Correlation coefficient and RMSE of surface temperature for model results and HYCOM data

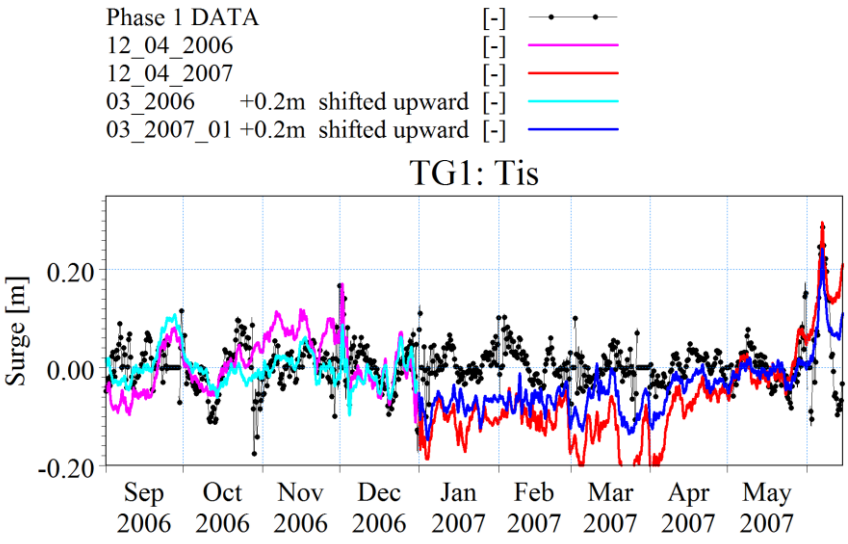

Figure 11. Comparisons on computed sea level change and filtered surge from Tis tide gauge

5. Results and discussion

Current speed and direction, sea surface elevation and temperature are the main outputs of the model which were compared to the collected data. An example comparison between the AW2 current profiler data and model results is presented in Figure 12. The figure provides comparison between surface currents and indicates that the model can reasonably reproduce the ocean current regime in Makran area. The oscillating nature of ocean currents is well reproduced. Current speeds are also reasonably simulated (a perfect match is not expected due to the extremely complex nature of the problem). The bottom panel in Figure 12 depicts the simulated temperature fluctuations near the seabed showing good consistency with the measured data.

Cyclone Gonu was an extreme event that took place in early June 2007. This event was recorded by the AW2 sensor. Figure 13 depicts comparisons between a selected section of the recorded data (black dots) and model results, demonstrating a great performance by the model in reproducing ocean currents along the Makran coastline. At the beginning of 2007 simulations were continued in two versions using two different temperature fields. The red line shows the results with the temperature field taken from the end of 2006 simulation, i.e., the simulation continued without any changes. The blue line was produced by a simulation whose initial temperature field was replaced with the data from C-GLORS (with other parameters such as velocity and water surface levels from the end of 2006).

As it appears in Figure 13, importing the temperature field from end of simulation at 2006 and using C-GLORS data, does not show a significant difference in the results of the model for 2007. This implies that the model's calculated temperature field in 2006 (by the end of one year simulation) is in a good consistency with the observed data.

The simulation was extended for 2008 using the same setting. Figure 14 illustrates a comparison between model results and ZarAbad data. Same patterns both in data and model results appear in this figure which implies that the simulations are adequately and consistently representing the oscillating currents along the Makran Coastline.

The model performance in simulating the Makran currents can also be seen through comparison between current speed simulated by the model and recorded by AW2, in the middle and bottom layers (Figure 15). As it appear in Figure 15, the trends of current speed variations are similar at surface, middle and bottom layers, however the magnitude of current speed is smaller near the bottom, which is expected for a mostly wind induced current.

Cyclone Gonu which is the most significant and devastating detected phenomenon in the region, was well simulated and this ensured that the modelling has achieved its engineering purposes. Figure 16 represents a snapshot showing the currents induced by Cyclone Gonu landing at Makran Coasts on 7th of June 2007.

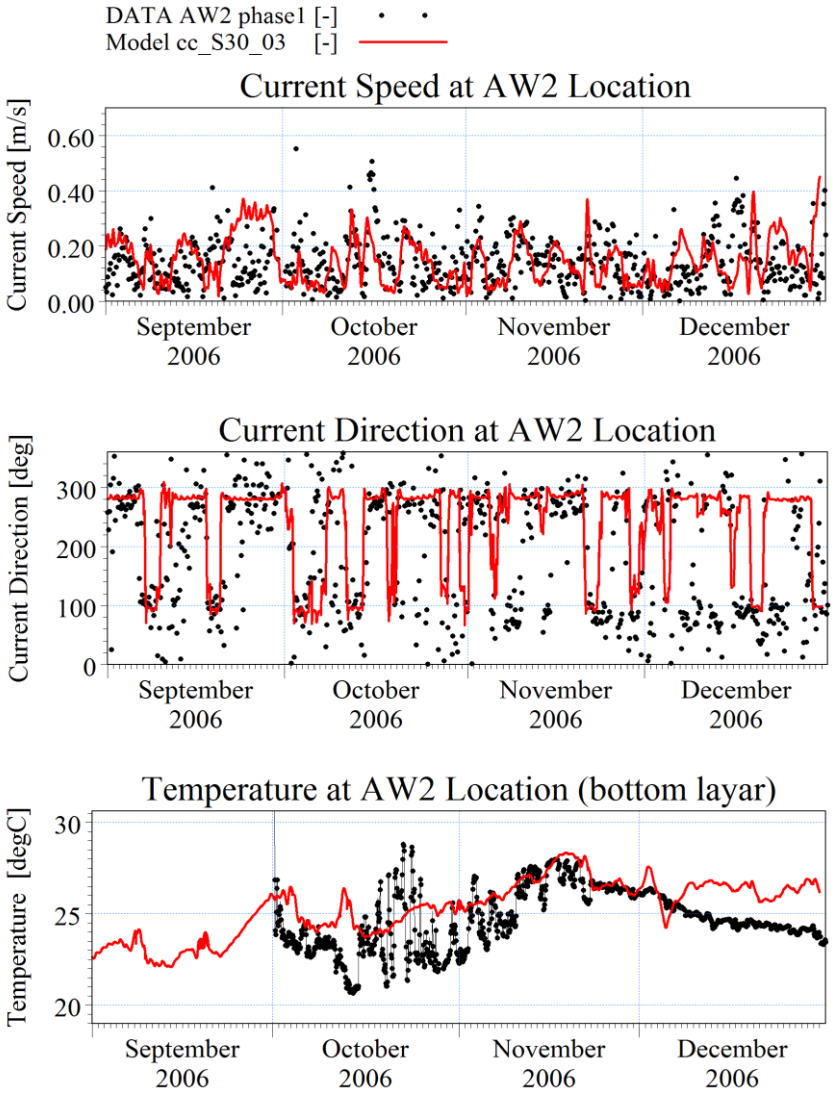

Figure 12. Comparisons between AW2 data (black) and model results (red).

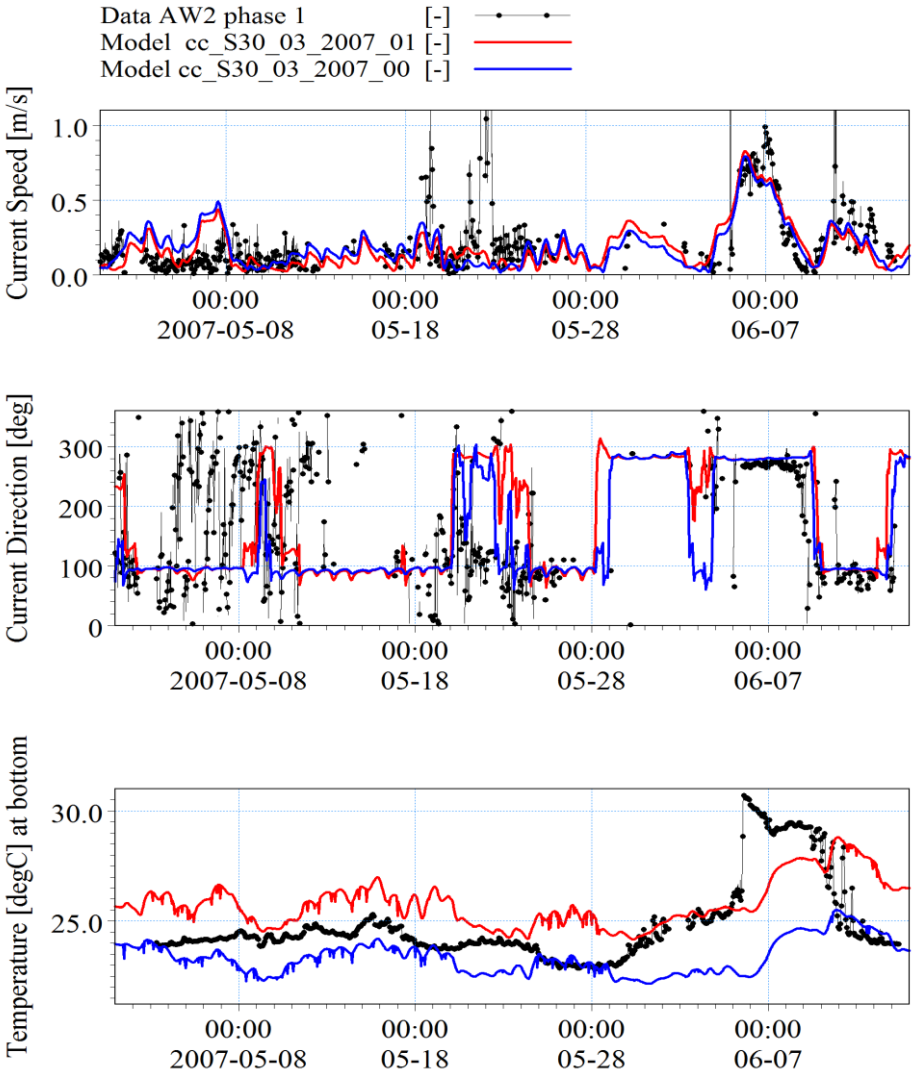

Figure 13. Comparisons between AW2 data (black) and model results (red) during cyclone Gonu.

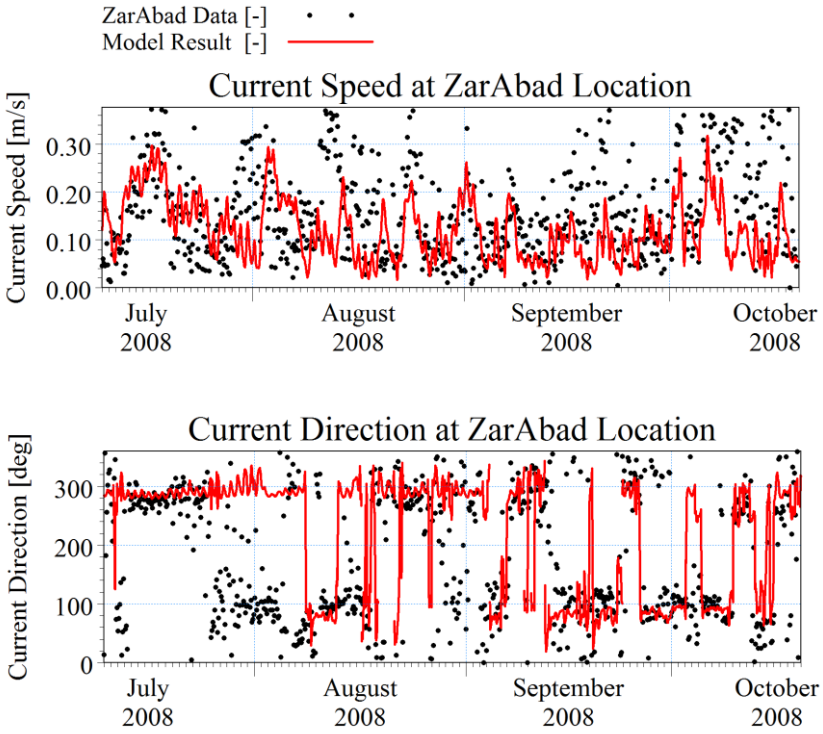

Figure 14. Comparisons between ZarAbad data (black) and model results (red).

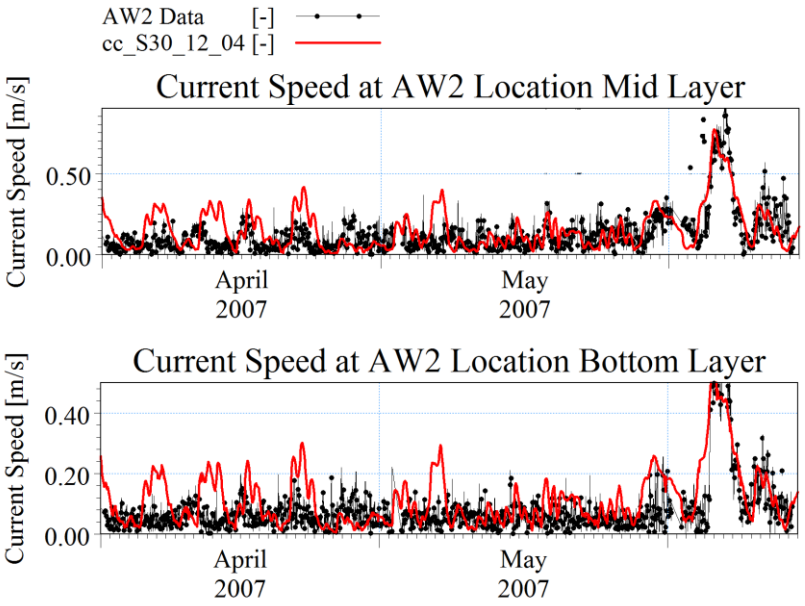

Figure 15. Comparisons on recorded (black) and simulated (red) current speed at AW2 in middle and bottom layers.

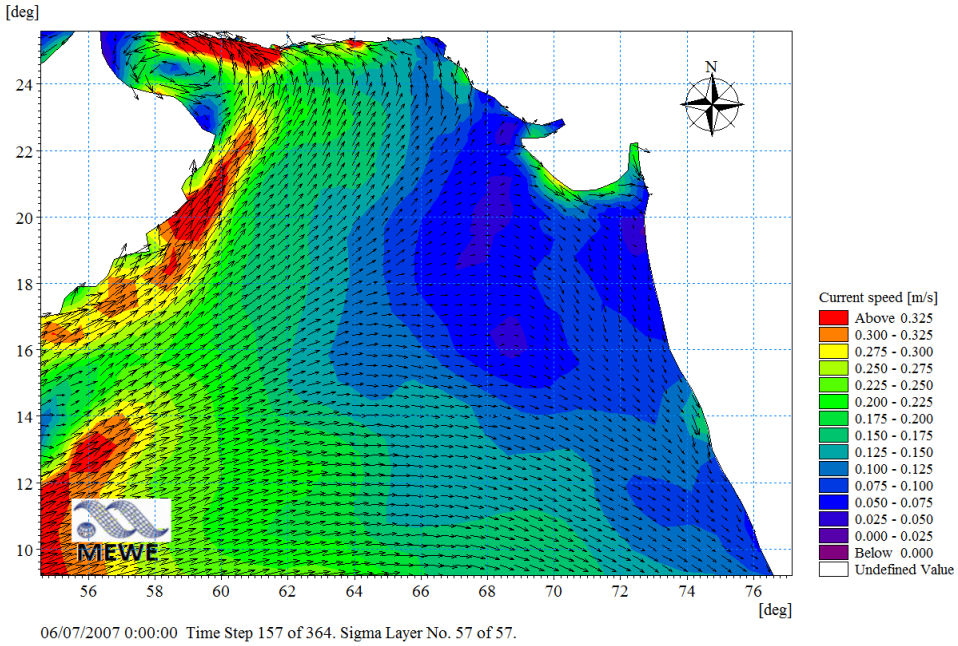

Figure 16. Currents induced by Cyclone Gonu on 7th of June 2007.

As a general ocean model, several criteria can be evaluated in order to validate to results including general current patterns, seasonal surface temperature filed and sea surface heights. Two monsoon seasons in the Northern Indian Ocean are characterized by the wind direction (Figure 17). While the trade wind below the Equator always blow towards the North-West, monsoon winds direction changes seasonally. Therefore two distinguished current pattern appear in this region.

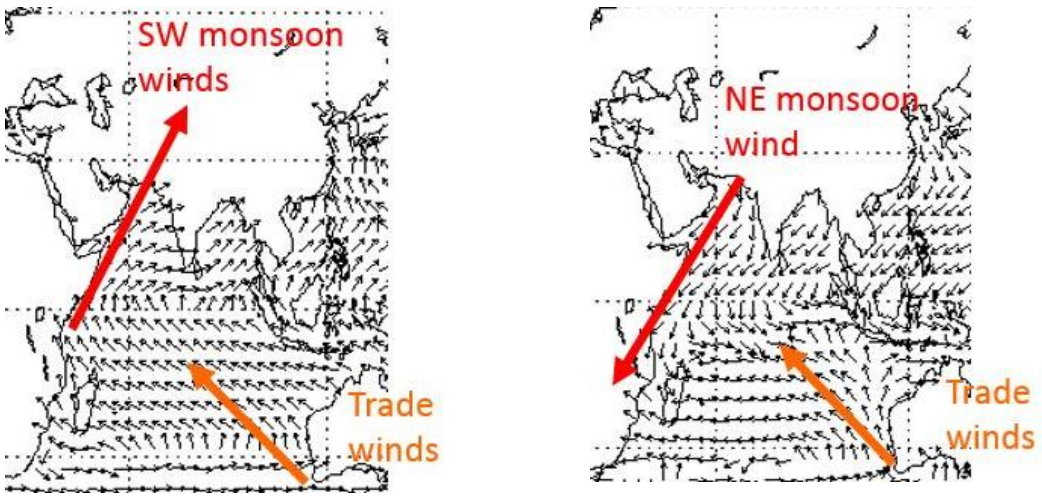

Figure 17. North Indian Ocean summer SW (left panel) and winter NE (right panel) monsoon winds

Figure 18 shows a comparison between currents simulated by the model in this research (green-dashed arrows) and satellite data analyzed by Shankar [4] (black-bold) arrows) for summer and winter monsoons. Nearest general current to the Makran Coasts is West Indian Coastal Currents (WICC) which in summer heads towards South-East and in winter towards

North-West. Somali Current (SC) adjusts it direction to the wind and subsequently is northward during summers and southward during winters. Winter Monsoon Current (WMC) passes through the South of India towards the West in winters. During summers, it is called SMC which its direction is eastward.

Geostrophic currents are oceanic flow in which the pressure gradient force is balanced by the Coriolis Effect. The direction of geostrophic flow is parallel to the isobars. Sea Surface Height (SSH) variations across the ocean are developed by variations in the air pressure, wind stress (surge) and variations in water density. SSH is a representative for pressure gradient in the ocean which forms isobars. Figure 19 illustrates SSH of the Northern Indian Ocean during winter extracted from ERDDAP [18] data in comparison with simulation results. Even though, subtle discrepancies are seen in the figure, the general SSH pattern seems to be well reproduced in the model.

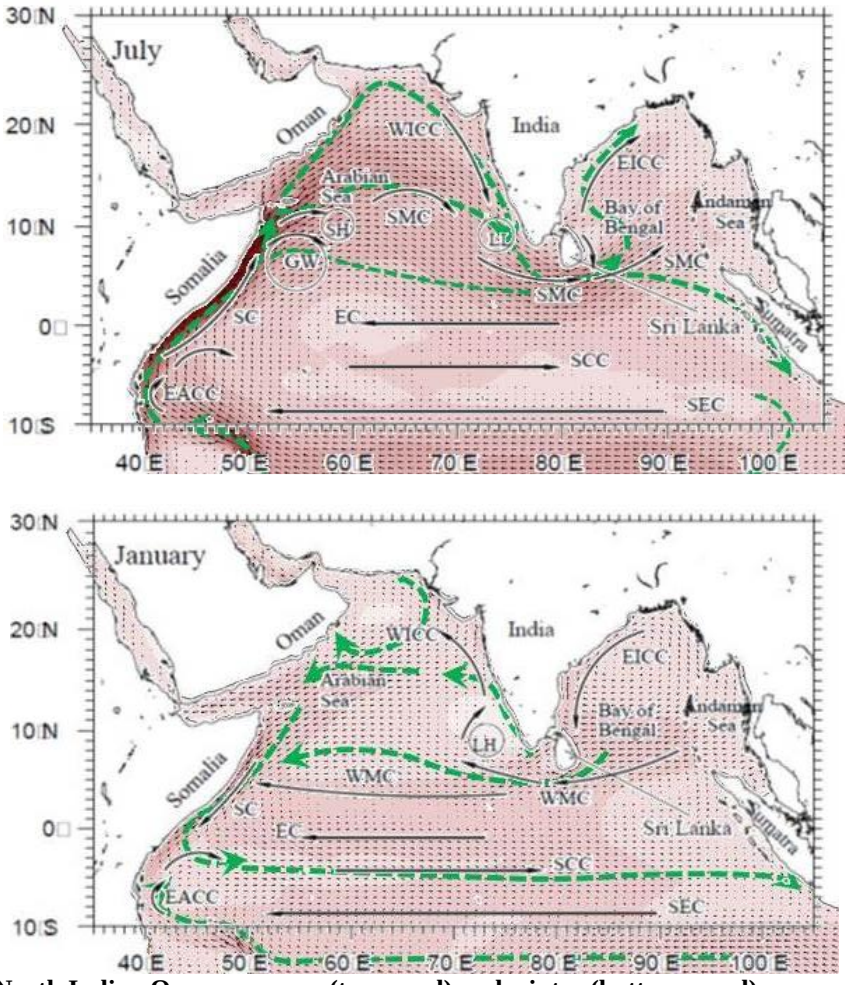

Figure 18. North Indian Ocean summer (top panel) and winter (bottom panel) monsoon currents.

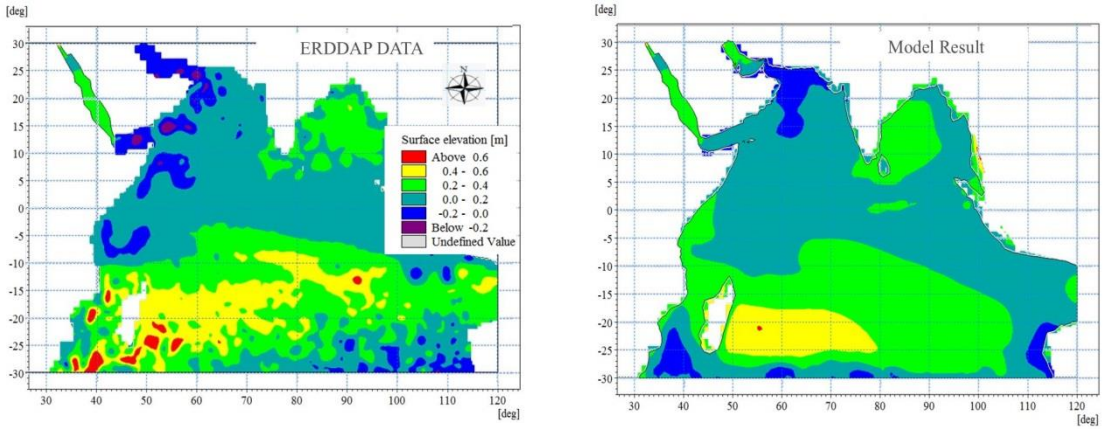

Figure 19. North Indian Ocean SSH; ERDDAP data (left panel) and model results (right panel)

Great Whirl (GW) which appears in Figure 18, an eddy which transports the water from Somali coasts towards east (offshore) reaches to its most developed stage in August. This causes coastal upwelling and appears as an abrupt drop in Sea Surface Temperature (SST) at its location. Figure 20 illustrates a comparison between Modis Satellite data analyzed by Savtchenko [19] and model results. Dashed circles locate the decreased SST caused by GW.

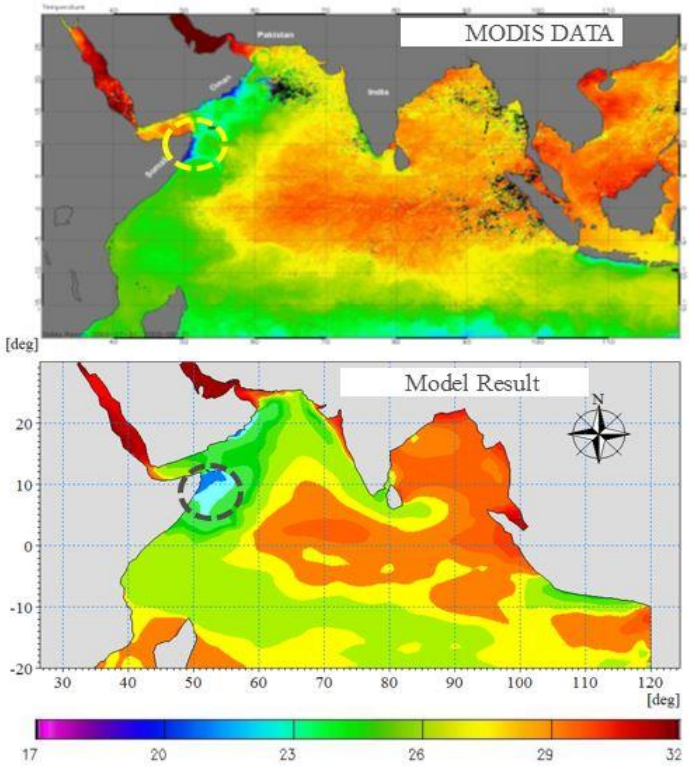

Figure 20. North Indian Ocean SST during summer monsoon; Modis Satellite data (top panel) and model results (bottom panel)

6. Conclusion

This paper presents the results of a 3D modelling effort for simulating the hydrodynamics of Makran ocean currents as well as their corresponding water level variations. Currents and sea levels in the Oman Sea are impacted by Indian Ocean. The data used for model calibration and verification were recorded in approximately 25 m and 19 m depth which fall in the shallower edge of the continental shelf just before the beginning of the transition zone to coastal currents. Moreover the capability of the model in reproducing the Northern Indian Ocean currents, SSH and SST was evaluated through comparisons with available data and literature.

7. References

1. Dibajnia, M., M. Jedari Attari, A. Bakhtiari, M.H. Nemati, S.A. Haghshenas (2016) Modelling of ocean currents and surge along the Iranian Makran coastline on the Oman Sea, *Proceedings of 12th ICOPMAS,* Tehran, Iran. pp. 51-52.
2. Jahad Water and Energy Research Company (JWERC) (2008) Study reports of "Monitoring and Modelling Studies of Parts of Sistan, Balouchestan and Boushehr Provinces", *Ports and Maritime Organization (PMO)*.
3. Darya Negar Pars Company (DNP) (2008) Study reports of "Waves and Currents data measurements in the vicinity of ZarAbad", *Iranian Fishery Organization (IFO)*.
4. Shankar, D. (2001) The monsoon currents in the north Indian Ocean. *Elsevier*
5. NASA (2011) Flat Map Ocean Current Flows with Sea Surface Temperatures (SST). *NASA/Goddard Space Flight Center Scientific Visualization Studio.* http://svs.gsfc.nasa.gov/goto?3821.
6. Lopez, Joseph, and Lakshmi Kantha (2000) "A Data-Assimilative Numerical Model of the Northern Indian Ocean." *American Meteorological Society.*
7. Aneesh, C.S. (2006) "Data Assimilation Experiments using an Indian Ocean General Circulation Model." *World Scientific*
8. Kurian, J., and P. N. Vinayachandran (20070 "Mechanisms of formation of the Arabian Sea mini warm pool in a high resolution *Ocean General Circulation Model.*" J. Geophys. Res. doi:10.1029/2006JC003631
9. Kawamiya, Michio, and Andreas Oschlies. 2003. "An eddy-permitting, coupled ecosystem-circulation model of the Arabian Sea: comparison with observations." *Journal of Marine Systems* 38: 221-257.
10. L'Hégaret. 2015. "Mesoscale variability in the Arabian Sea from HYCOM model results and observations: impact on the Persian Gulf Water path." *Ocean Sci. Discuss.*
11. Argo data management (2013) "Argo user's manual." (Ifremer). doi:10.13155/26387.
12. U.S. Navy HYCOM (2015) Real-time 1/12° Global HYCOM Nowcast/Forecast System. Prod. HYCOM Consortium for Data-Assimilative Ocean Modeling. *Naval Research Laboratory*. http://www7320.nrlssc.navy.mil/GLBhycom1-12/skill.html.
13. Tartinville, B., E. Deleersnijder, P. Lazure, R. Proctor, K. Ruddick and R. Uittenbogaard. (1998) A coastal ocean model intercomparison study for a three-dimensional idealized test case, *Applied Mathematical Modelling,* pp. 165-182.
14. CMCC (2014). The CMCC Global Ocean Physical Reanalysis System *C-GLORS.*
15. Ghader, S., D. Yazgi, S.A. Haghshenas, A. Razavi Arab, M. Jedari Attari, A. Bakhtiari and H. Zinsazboroujerdi (2016). Hindcasting tropical storm events in the Oman sea. *Journal of Coastal Research.* 75. 1087-1091.

16. CCAR (2013) Reconstructed Sea Level Version 1. *Prod. Boulder University of Colorado.* http://podaac.jpl.nasa.gov/dataset/RECON_SEA_LEVEL_OST_L4_V1.
17. Amante, & Eakins. (2009). ETOPO1 1 Arc-Minute Global Relief Model: Procedures, Data Sources and Analysis. *NOAA Technical Memorandum* NESDIS NGDC 24. National Geophysical Data Center, NOAA. doi:10.7289/V5C8276M
18. ERDDAP (2017) Easier access to scientific data, https://coastwatch.pfeg.noaa.gov/erddap/index.html
19. Savtchenko (2004) An assessment of the Indian Ocean, Monsoon, and Somali Current using NASA's AIRS, MODIS, and QuikSCAT data, http://disc.sci.gsfc.nasa.gov/